Hindawi Publishing Corporation
Science and Technology of Nuclear Installations
Volume 2011, Article ID 574514, 13 pages
doi:10.1155/2011/574514

Research Article

CFD Recombiner Modelling and Validation on the H_2-Par and Kali-H_2 Experiments

Stéphane Mimouni,[1] Namane Mechitoua,[1] and Mehdi Ouraou[2]

[1] *R&D Division, Electricité de France, 6 Quai Watier, 78400 Chatou, France*
[2] *INCKA, 85 avenue Pierre Grenier, 92100 Boulogne, France*

Correspondence should be addressed to Stéphane Mimouni, stephane.mimouni@edf.fr

Received 14 March 2011; Revised 29 April 2011; Accepted 6 May 2011

Academic Editor: Giorgio Galassi

A large amount of Hydrogen gas is expected to be released within the dry containment of a pressurized water reactor (PWR), shortly after the hypothetical beginning of a severe accident leading to the melting of the core. According to local gas concentrations, the gaseous mixture of hydrogen, air and steam can reach the flammability limit, threatening the containment integrity. In order to prevent mechanical loads resulting from a possible conflagration of the gas mixture, French and German reactor containments are equipped with passive autocatalytic recombiners (PARs) which preventively oxidize hydrogen for concentrations lower than that of the flammability limit. The objective of the paper is to present numerical assessments of the recombiner models implemented in CFD solvers NEPTUNE_CFD and Code_Saturne. Under the EDF/EPRI agreement, CEA has been committed to perform 42 tests of PARs. The experimental program named KALI-H_2, consists checking the performance and behaviour of PAR. Unrealistic values for the gas temperature are calculated if the conjugate heat transfer and the wall steam condensation are not taken into account. The combined effects of these models give a good agreement between computational results and experimental data.

1. Introduction

During a design-basis accident (DBA) or a severe accident (SA) in a nuclear power plant, certain chemical reactions may produce hydrogen (hydrogen is produced from the oxidation of zirconium sheaths and structures of fuel elements during the phase of core degradation), in such a way that hydrogen and oxygen volumetric concentrations may exceed the lower flammability limits (LFLs). The hydrogen risk in a nuclear power plant may be defined as the risk of hydrogen combustion in the containment building which represents a threat to the integrity of the confinement due to pressure and temperature levels. The nuclear safety is based on the concept called "defence-in-depth" that consists of a hierarchical deployment of different levels of equipment and procedures to maintain the efficiency of the physical barriers.

The transport and distribution of hydrogen inside the containment or the different compartments are critical phenomena to determine the kinetic and the nature of combustion. The prediction of stratification phenomena and location of hydrogen pockets are essential to assess the hydrogen risk and then to optimise the hydrogen hazard mitigation system.

Among the different safety systems for limiting the pressure increase during the course of the accident and the impact of possible combustion (deflagration), French and German PWR reactors have three types of mitigation means.

(i) Sprinkler systems: the injected water droplets cool the containment and lower the pressure by condensing steam on the droplets. They also promote mixing of gas and rapidly break possible stratifications of the lightest gases.

(ii) The walls of the containment building and metal structures also play an important role from a thermal viewpoint. The walls, significantly cooler than the gas, condense the water vapor in the gas mixture and thus limit the pressure increase in the containment. Furthermore, the temperature difference between fluid and walls generates a convection loop, enhancing the mixing of gases of different density.

(iii) The passive autocatalytic recombiners (PAR): their role is to proactively oxidize hydrogen for preventing its accumulation in the containment. The catalytic recombiners initiate a controlled combustion, which is similar to a slow deflagration.

A catalytic recombiner consists of a vertical channel or stack equipped with a catalyst bed in the lower part. In case of an accident, the catalyst is in contact with the gas mixture of the containment. Hydrogen molecules coming into contact with the catalyst surface are reacted with oxygen to form steam. The heat of the reaction at the catalyst surface causes a buoyancy-induced flow accelerating the inflow rate and thereby feeding the catalyst with a large amount of hydrogen that ensures high efficiency of recombination. The natural air circulation ensures a continuous air supply to the catalytic recombiner. This effect is increased by the height of the chimney, the inlet free area, and the fast heat up of the catalytic plates.

Catalytic recombiners favour the chemical reaction $H_2 + (1/2)O_2 \rightarrow H_2O$ by lowering the activation energy threshold so that the reaction takes place at low temperature and concentration. The active catalyst materials include the noble metals platinum or palladium. The cover of the housing at the top protects the catalyst against direct spray of water and aerosol deposition. A catalytic recombiner is considered as"passive" because such a device is self-starting and self-feeding, and requires no external energy. Catalytic recombiners can start up with hydrogen fraction equal to about 2%.

This paper focuses on numerical assessments of PAR's modeling implemented in CFD solver Code_Saturne and CMFD solver NEPTUNE_CFD [1–6]. It is organized as follows. The first part describes briefly the NEPTUNE_CFD code [7]. Next, the gas dynamic model implemented in Code_Saturne is described [8]. The second part presents the LP manufacturer's models of recombiners and their implementation in these codes. The third part concerns the numerical assessments upon the H_2-PAR and KALI-H_2 experiments and the discussion of the results.

2. Two-Phase Flow Model Used in NEPTUNE_CFD

The solver belongs to the well-known class of pressure-based methods. It is able to simulate multi-component multiphase flows by solving a set of three balance equations for each field (fluid component and/or phase) [9]. These fields can represent many kinds of multiphase flows: distinct physical components (e.g., gas, liquid, and solid particles); thermodynamic phases of the same component (e.g., liquid water and its vapour), distinct physical components, some of which split into different groups (e.g., water and several groups of different diameter bubbles); different forms of the same physical components (e.g., a continuous liquid field, a dispersed liquid field, a continuous vapour field, and a dispersed vapour field). The solver is implemented in the NEPTUNE software environment [7, 10], which is based on a finite volume discretization, together with a collocated arrangement for all variables. The data structure is totally face-based which allows the use of arbitrary-shaped cells (tetraedra, hexaedra, prisms, pyramids, etc.) including nonconformal meshes.

The main interest of the numerical method is the so-called "volume fraction-pressure-energy cycle" that ensures mass and energy conservation and allows strong interface source term coupling [11].

Mass balance equations, momentum balance equations and total enthalpy balance equations, are solved for each phase. The gas turbulence is taken into account by the classical k-ε model. The droplet diameter evolution is calculated from an equation of transport on the density of drops. Additional equations are added to take into account the noncondensable gases (air and hydrogen). Concerning the interfacial momentum transfer terms, the only force exerted on droplet is the drag force. Small droplets stick to the wall and large drop slide along the wall under the competition between the surface tension and the gravity force. As a consequence, the gas velocity near the wall does not tend to zero but to the droplets velocity because of the drag force. This is a major difference between single-phase and two-phase flow approach [12]. Concerning the heat and mass transfer between droplets and the wall, it is based on the balance of heat and mass transfer between a drop and the gas mixture surrounding the drop using the correlations of Frössling/Ranz-Marshall which are of widespread use [13].

The model of drop-wall interaction which was developed and implemented is written as a symmetric extension of the nucleate boiling model at the wall, and uses as a starting point the model of mass transfer in the core flow. To establish this model, we made the following assumptions:

(i) the drops which accumulate on the walls take a hemispherical form;

(ii) there is no nucleate boiling inside the drops at the wall;

(iii) the drops which impact the walls successively see a stage of cooling (resp., heating) and a stage of condensation (resp., evaporation);

(iv) the droplets stick to the wall (no rebound), or slide along the wall.

The total heat flux exchanged between the wall and the flow is split into four terms:

(i) φ_{C1} a single-phase flow convective heat flux at the fraction of the wall area unaffected by the presence of droplets (heat transfer between the gas and the wall);

(ii) φ_{C2} a single-phase flow convective heat flux at the fraction of the wall area affected by the presence of a liquid film (heat transfer between the liquid film and the wall);

(iii) φ_{Th} a single-phase flow heat flux to decrease (resp., increase) the droplet temperature and reach the wall temperature (resp., the saturation state) (heat transfer between the droplets and the wall);

(iv) φ_E a condensation (resp. vaporisation) heat flux.

Details can be found in [14]. An extensive validation process has been achieved in [12] against the COPAIN experiment and mesh sensitivity has been found acceptable.

In fact, a particular model is developed to reduce the sensitivity to the mesh refinement, for example, the gas temperature and the gas velocity in the nearest cell at the wall depend on the size of the cell with a volume finite method. As a consequence, on one hand, we use the value calculated in the cell and given by the direct resolution of the momentum equation (gas velocity) and the energy equation (gas temperature). On the other hand, we use standard wall functions for the gas velocity and temperature at a nondimensional distance to the wall. The combination of these values provides a weakly dependent value for the gas velocity and temperature near the wall, and these values are the input of the model of heat and mass transfer at the wall.

3. Homogeneous Gas Dynamic Model Used in Code_Saturne

The motion, the distribution of gases, and heat transfer in containment enclosures can be described by the general momentum, partial masses, and energy conservation equations.

The predominant physical phenomena driving the motion, the distribution, and heat transfer of fluids within containment enclosures are follows.

Mixing and/or segregation of gas whose velocity, density, and temperature are different.

(i) "Swelling" of containment: the compressibility of gas is taken into account, even if the flow velocities are low.

(ii) Laminar and controlled combustion of hydrogen in recombiners, in order to limit the concentration of this gas.

(iii) Condensation of steam on cold structure surfaces, which has the main effect of limiting the pressure rise.

The general momentum, partial masses, and energy conservation equations describing these phenomena can be simplified, and stiffness due to the presence of physics having very different characteristic length and time scales can be removed or relaxed.

The used turbulence model for containment applications is the standard k-epsilon one, supplemented by wall log laws for taking into account the turbulent friction and gaseous heat transfer between the fluid and the surrounding structures.

3.1. Low Mach Number Approximation. The flows are mainly low Mach number flows, whose motion is predominantly driven by free convection. A low Mach number model can be implemented in a pressure correction-based solver usually used for incompressible or steady dilatable flows, as Code_Saturne [8]. A spatial filtering of acoustic waves leads to separate the static pressure P into a uniform time-dependant thermodynamic pressure $P_{\text{th}}(t)$ and a mechanical pressure $p(x,t)$:

$$P = P_{\text{th}}(t) + p(x,t); \quad P_{\text{th}} \gg \left| p(x,t) \right|. \tag{1}$$

The general motion conservation equation of the mixture

$$\frac{\partial \rho \underline{V}}{\partial t} + \operatorname{div}\Big[\underline{V} \otimes \rho \underline{V} - \mu_{\text{tot}}\left(\nabla \underline{V} + {}^{t}\nabla \underline{V}\right) + \left(\frac{2}{3}\mu_{\text{tot}} \operatorname{div} \underline{V} + \frac{2}{3}\rho k + P\right)\underline{\underline{I}}\Big] = \rho \underline{g} + \Gamma_{\text{cond}} \underline{V}_I, \tag{2}$$

associated with the supplementary approximations concerning the mechanical pressure and taking into account mean hydrostatic pressure

$$p(x,t) \equiv p(x,t) + \frac{2}{3}\mu_{\text{tot}} \operatorname{div} \underline{V} + \frac{2}{3}\rho k + \rho_0 g z \quad \text{with } \rho_0 \equiv \frac{\int \rho \, d\Omega}{\Omega_0}, \tag{3}$$

then becomes

$$\frac{\partial \rho \underline{V}}{\partial t} + \operatorname{div}\left[\underline{V} \otimes \rho \underline{V} - \mu_{\text{tot}}\left(\nabla \underline{V} + {}^{t}\nabla \underline{V}\right)\right] + \nabla p = (\rho - \rho_0)\vec{g} + \Gamma_{\text{cond}} \underline{V}, \tag{4}$$

where ρ, $\underline{V}$, μ_{tot}, p, ρ_0, Γ_{cond} stand, respectively, for the mixture density, the mixture velocity vector, the total dynamic viscosity (including the turbulent viscosity deduced from the k-ε turbulence model), the mechanical pressure, the averaged density, the gravity acceleration, and the condensation sink term.

Thanks to the low Mach number approximation, the mechanical pressure is neglected for the computation of density, through the thermal equation of state:

$$\rho = \frac{P_{\text{th}}}{RT \sum_k Y_k / M_k}, \tag{5}$$

where R, T, Y_k, and M_k stand, respectively, for the perfect gas constant, the absolute temperature (in Kelvin), and the mass fractions of the different gases contained in the reactor building during a severe accident (oxygen, nitrogen, steam, and hydrogen).

The supplementary unknown P_{th} is solved, using integral forms over the entire domain Ω_0 of mass or enthalpy equations, written below.

$$\frac{\partial}{\partial t}\int_{\Omega_0} \rho \, d\Omega = \int_{\Omega_0} \Gamma_{\text{cond}} d\Omega - \int_{\partial\Omega_0} \rho \underline{V}\underline{n} \, dS$$

or

$$\frac{dP_{\text{th}}}{dt}\Omega_0 = -\frac{\partial}{\partial t}\int_{\Omega_0} \rho h \, d\Omega - \int_{\partial\Omega_0}\left[\rho \underline{V} h - \left(\frac{\mu_t}{\sigma_t} + \frac{\lambda}{C_p}\right)\nabla h\right] n \, dS + \int_{\Omega_0} \rho S_h d\Omega. \tag{6}$$

3.2. Energy Equation. The enthalpy equation of the mixture is quite complex and contains several terms. The body forces, the viscous constraint contributions, and the supplementary terms due to the presence of more than two different species are negligible, when compared to the convective and turbulent transport contributions. For low Mach number flows, the kinetic energy remains small when compared to the thermal energy. On the other hand, the unsteady contribution of the thermodynamic pressure is conserved, as it plays a key role in the pressure rise in the containment.

The Fourier laminar and turbulent conduction term is directly written according to the enthalpy variable through the linearized relation

$$\lambda \frac{\partial T}{\partial x_j} = \frac{\lambda}{C_p} \frac{\partial h}{\partial x_j}, \tag{7}$$

where λ and C_p stand, respectively, for conductivity and specific heat of the mixture.

The enthalpy equation is written in the following form:

$$\frac{\partial \rho h}{\partial t} + \operatorname{div}\left[\rho \underline{V} h - \left(\frac{\mu_t}{\sigma_t} + \frac{\lambda}{C_p}\right)\nabla h\right] = \frac{dP_{\text{th}}}{dt} + \Gamma_{\text{cond}} h_{\text{steam}} - \rho \cdot E \cdot \frac{dm_{\text{H}_2}}{dt}, \tag{8}$$

where h stands for the sensitive enthalpy, defined as $h \equiv \int_{T_0}^{T} C_p dT$, C_p is the mixture-specific heat.

Then, in presence of exothermic chemical reactions, due to the combustion of hydrogen by the recombiners, the transformation of formation enthalpy into sensitive enthalpy is taken into account through a source term proportional to the sensitive enthalpy E released by the chemical reactions and to the chemical reaction speed dm_{H_2}/dt. The same term is implemented in the energy equation in the NEPTUNE_CFD code.

We recall that the formation enthalpies and reaction heat E at ambient temperature are

$$h^0_{\text{H}_2}(T_0) = h^0_{\text{He}}(T_0) = h^0_{\text{O}_2}(T_0) = h^0_{\text{N}_2}(T_0) = 0,$$
$$h^0_{\text{H}_2\text{O,vap}}(T_0) = -13.4\,\text{MJ/kg}; \quad E = 122\,\text{MJ/kg}. \tag{9}$$

The heat transfer due to condensation at the walls is modelled through a sink term proportional to the steam mass reduced into liquid water Γ_{cond} and the latent heat L_{cond}.

In the following sections, calculations performed with Code_Saturne do not take into account the condensation phenomena at wall.

4. Recombiners Modelling in Both Codes

In this study we will use the following rate for the reaction $H_2 + (1/2)O_2 \rightarrow H_2O$:

$$\frac{dm_{\text{H}_2}}{dt} = -\frac{\eta}{1000} \cdot X \cdot (AP + B) \cdot \tanh\left[100\left(X - X_{\text{H}_2,\text{min}}\right)\right] \quad \text{if } X > X_{\text{H}_2,\text{min}}$$
$$\frac{dm_{\text{H}_2}}{dt} = 0, \quad \text{if } X < X_{\text{H}_2,\text{min}}, \tag{10}$$

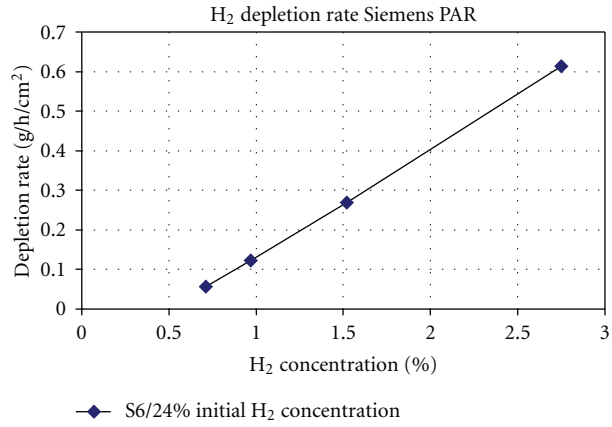

Figure 1: H_2 depletion rate.

where dm_{H_2}/dt stands for the recombined mass rate of H_2 (kg/s), and where X_{min} is such that

$$X_{\text{min}} = \min\left(X_{\text{H}_2}; 2X_{\text{O}_2}; 0.08\right), \tag{11}$$

with X the molar fraction. Moreover, P is the pressure in bars, and η a parameter interpreted as the recombiner output, and allowing to take into account the decrease of the efficiency of the recombiner for the weak concentrations of oxygen:

$$\eta = 1, \quad \text{if } X_{\text{H}_2} < X_{\text{O}_2},$$
$$\eta = 0.6, \quad \text{if } X_{\text{H}_2} > X_{\text{O}_2}. \tag{12}$$

A and B are given by SIEMENS for the FR90/1-150 PAR and take, respectively, the values 0.48×10^{-3} kg/s/bar and 0.58×10^{-3} kg/s [3]. For another SIEMENS recombiner, only the values of A and B are changed.

Moreover $X_{\text{H}_2,\text{min}} = 0.005$.

An important point to underline is that the hydrogen depletion rate is a semiempirical relation, based on experimental measures made at the inlet and at the outlet of the recombiner. In other words, the rate given by this expression is a global rate on the whole recombiner.

The reaction $H_2 + (1/2)O_2 \rightarrow H_2O$ is exothermic. The released heat is equivalent to 122 MJ/kg of H_2 burnt. The energy produced is released in the vicinity of the plates only if the reaction occurs, and is a function of the rate of H_2 burnt.

5. Mass Conservation Equation in Both Codes

The mass conservation equations are written as below:

(i) the global mass equation, containing the sink term of wall condensation:

$$\frac{\partial \rho}{\partial t} + \operatorname{div}(\rho \underline{V}) = \Gamma_{\text{cond}} \tag{13}$$

(Figure 1),

(ii) the conservation equations of noncondensable gases, containing the slow combustion sink terms due to the recombiners:

$$\frac{\partial \rho_1 Y_{O_2}}{\partial t} + \operatorname{div}\left(\rho_1 \underline{V} Y_{O_2} - \rho_1 D \nabla Y_{O_2}\right) = \Gamma_{O_2} = \rho_1 \frac{M_{O_2}}{2M_{H_2}} \frac{dm_{H_2}}{dt},$$

$$\frac{\partial \rho_1 Y_{H_2}}{\partial t} + \operatorname{div}\left(\rho_1 \underline{V} Y_{H_2} - \rho_1 D \nabla Y_{H_2}\right) = \Gamma_{H_2} = \rho_1 \frac{dm_{H_2}}{dt},$$

$$\frac{\partial \rho_1 Y_{N_2}}{\partial t} + \operatorname{div}\left(\rho_1 \underline{V} Y_{N_2} - \rho_1 D \nabla Y_{N_2}\right) = \Gamma_{N_2} = 0, \tag{14}$$

(iii) the relation for obtaining the condensable gas (steam) from the concentration of the other gases:

$$Y_{H_2O} = 1 - Y_{O_2} - Y_{N_2} - Y_{H_2}, \tag{15}$$

Finally, very similar numerical method and physical modelling are implemented in both codes by the same team. The main difference is that NEPTUNE_CFD can handle multiphase flows. But the H_2-PAR and KALI-H_2 test can be modelled by a single-phase approach. As a consequence, Code_Saturne and NEPTUNE_CFD will be used in the following sections.

6. H_2-PAR Test Case

To validate the recombiner model, two H_2-PAR testing programs were carried out and the results were compared with experimental data. The experimental device consists of a sealed bag of flexible material to an approximate volume of 7.6 m^3, which contains a Siemens FR90/1-150 type recombiner of 0.2 m length, 0.166 m wide and 1.03 m in height. The volume of this pocket is not constant over time, the variation being of the order of one m^3. The atmosphere is initially composed of air and water vapor. Hydrogen is introduced at the base of the plant for a specified period. Hydrogen concentrations were measured by gas chromatography every minute at different locations (in particular, at recombiner inlet and outlet). They are then averaged over the whole field.

The computational domain is modelled by a cube and does not take into account the change in volume of the chamber (a flexible pouch; Figures 2 and 3). The mesh contains 6859 cells, with 19 cells in each direction of space. The recombiner volume is taken into account with approximately 40 cells.

The operating conditions of test-E2 and E19 are summarized below (Table 1).

At Inlet. E2-bis test: the mass flowrate is successively 1.3030×10^{-3} kg·s^{-1} (between 0 and 10 s), 4.3435×10^{-4} kg·s^{-1} (between 10 and 25 s), 1.9743×10^{-4} kg·s^{-1} (between 25 and 36 s). The hydrogen mass fraction is equal to 1 and the gas temperature is 85°C.

E19 test: the mass flowrate is 0.18×10^{-3} kg·s^{-1} between 0 and 200 s. The hydrogen mass fraction is equal to 1 and the gas temperature is 70°C.

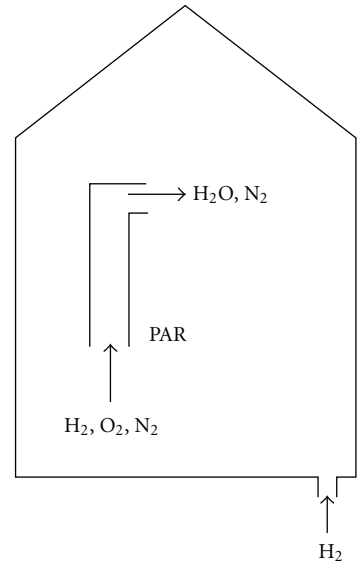

Figure 2: H_2-PAR test case.

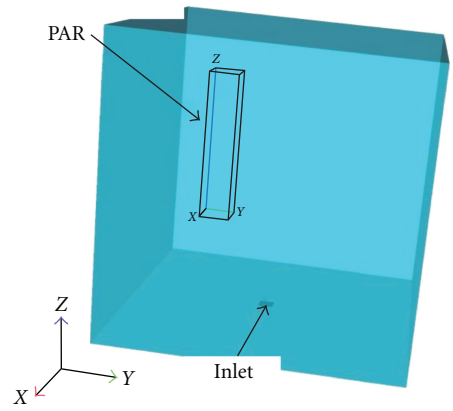

Figure 3: H_2-PAR test: computational domain.

Table 1: Initial conditions—H_2-PAR test.

	Essai E2-Bis	Essai E19
O_2 molar fraction	0.0828	0.1403
N_2 molar fraction	0.3112	0.5274
H_2O molar fraction	0.6054	0.3323
H_2 molar fraction	0	0
Temperature	85°C	70°C
Pressure (Pa)	101300	101300

Walls. Adiabatic conditions.

The differences in density, generated by the combustion of hydrogen, create a natural convection loop that enhances the mixing at the same level and above recombiner. Moreover, cold stratified zone below the recombiner is calculated. The schematic modelling performed here may be representative of what can happen in the real case of the reactor

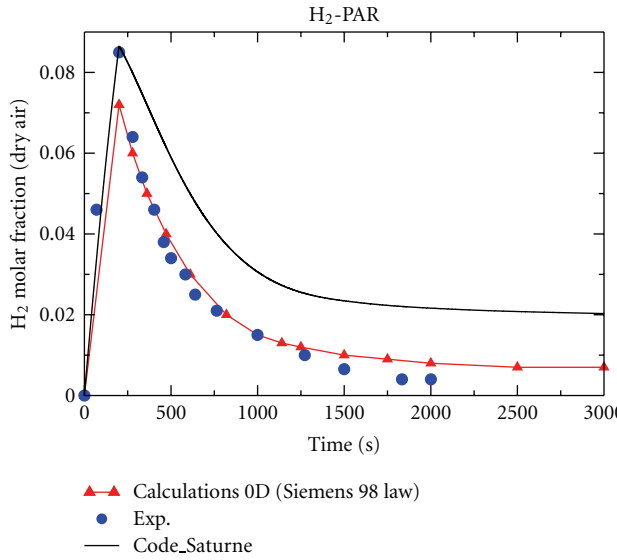

Figure 4: E19 test—time evolution of hydrogen molar fraction.

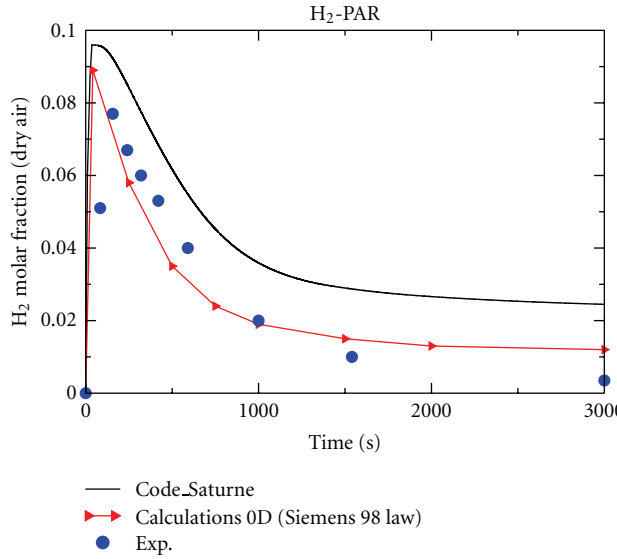

Figure 5: E2bis test—time evolution of hydrogen molar fraction.

building. Two opposing phenomena are in competition: the recombiner promote the controlled combustion of hydrogen, but according to their position in the enclosure, may also promote the creation of stratified layers of gas, "resistant" to the mix. Figures 4 and 5 show the time evolution of the overall concentration of hydrogen dry gas (deduced from the volume fraction of vapour) measured in the chamber and calculated with Code_Saturne and scenario MAAP code with the 0D model [15]. The continuous curves represent the results obtained when the source term is distributed over all the meshes representing the recombiner volume. The source term is calculated in each mesh of the recombiner with the local concentration of hydrogen and oxygen, weighted by the volume of the mesh on the overall recombiner volume.

The manufacturer correlation for the hydrogen depletion rate is dedicated to scenario code (like MAAP) with 0D model, and the challenge is to find a method to implement this manufacturer correlation in a CFD code. Figures 4 and 5 show that the method described in the paper allows to reach a reasonable agreement with the experimental data without fully solving the recombination processes. In fact, if we solve the recombination processes accurately and locally, the PAR component when integrated with containment mixing calculations would result in a large number of mesh elements which may take large computational times to solve the problem.

The exercise carried out in this paragraph remains modest compared to the real complexity of the operation of a catalytic recombiner. But the goal here is to qualitatively

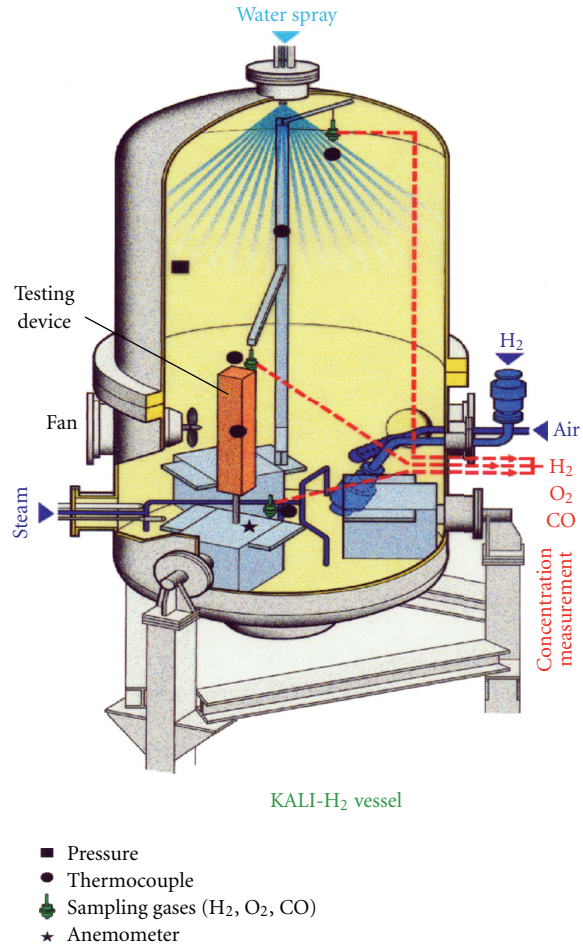

Figure 6: KALI-H_2 test.

reproduce the local effects induced by the operation of recombiner.

7. KALI-H_2 Test

7.1. KALI-H_2 Experiments. To test the catalytic capability of the SIEMENS recombiner model FR90/1-150, we used the KALI vessel. This 15.6 m^3 vessel (4.6 m height and 2.1 m of diameter) is able to withstand a pressure of 12 bar. The recombiner is located close to the wall, at the bottom of the vessel.

The vessel is connected with specific systems: steam injection system, hydrogen injection system,n and cold water system (Figures 6 and 7). Figures 8 and 9 show measurements location.

The vessel is also equipped with a fan to avoid any stratification during the hydrogen injection and also to start with a homogeneous mixture (it is stopped 45 s after the beginning of the hydrogen injection). Since the test facility cannot accommodate a full-size recombiner unit, a small-size segment model was tested. Figure 9 shows that the small-size recombiner is made of 15 vertical plates of 15 cm height, 15 cm depth, and 0.12 mm thickness with 1 cm spacing between them.

7.2. Numerical Setup. The recombiner was represented as a box of which the dimensions were the ones from the outside of the recombiner. Plates are not modeled.

In our global approach, source terms are distributed over the meshes representing the active recombiner volume containing the vertical plates. Source terms are calculated in each mesh of the recombiner with the local concentration of hydrogen and oxygen, weighted by the active recombiner volume.

The simulations couple the two-phase flow and the solid heat conduction within the wall vessel. The wall condensation of vapor is taken into account with NEPTUNE_CFD code. In fact, in a real situation, heat transfer to the wall and condensation result in an enhanced mixing of the atmosphere. In order to underline these aspects, Code_Saturne simulations are performed with the artificial assumption of adiabatic walls and without wall condensation.

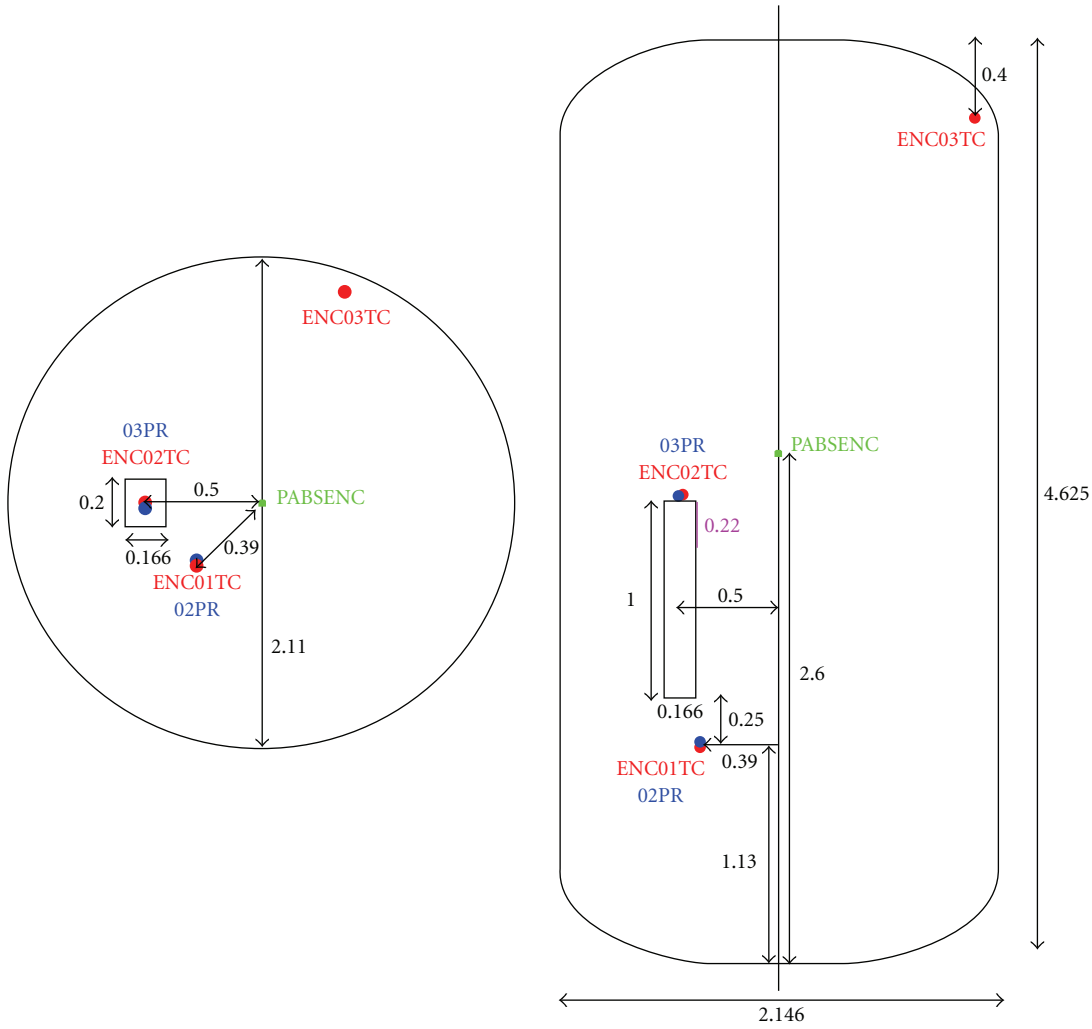

Figure 7: Sketch of the computational domain of the KALI-H_2 test.

The initial conditions of the test 008 are the following:

(i) pressure: 3.25 bars,

(ii) temperature: 30°C (303 K),

(iii) 4% of H_2,

(iv) 96% of air,

(v) no steam (water) initially.

Successive stages have to be considered for calculations: mixing of the gases with a fan device occurs every 900 s for 120 s. Moreover, an initial mixing is present during the first 120 s of the test. The successive stages of the simulation are given in Figure 10.

We assume that the end of the mixing leads to a homogeneous gas mixing in the whole KALI-H_2 vessel. Hence, the initial thermal-hydraulics properties of the calculations are taken at this time: homogeneous repartition of gas and temperature. The simulation carries on up to the second phase of mixing (900 s → 1020 s of test time). To take into account the homogenisation stage by the fan device, we reinitialise the computational values with averaged values calculated in the entire computational domain. This operation begins at the half of the duration of homogenisation process. Nevertheless, values inside the recombiner remain unchanged.

Thus the mixing stage is simplified, but avoids taking into account the fan device for which few data are available. Then, calculations continue up to a second point of experimental recording (1080 s).

The number of cells is about 112000. The time step corresponds to CFL = 1.

7.3. Results and Discussion. The sensitivity to the turbulence modelling has been investigated with NEPTUNE_CFD code, and calculations with three turbulent models (k-epsilon model, R_{ij}-epsilon model [16], and laminar model) have been performed. The results are quite similar which means that the turbulence modelling does not affect the results significantly. In KALI-H_2 test, the turbulence modelling is not of relevant interest because the fan device leads to a homogeneous mixing in the vessel. Turbulent effects lead also to a homogeneous mixing in the vessel but this is

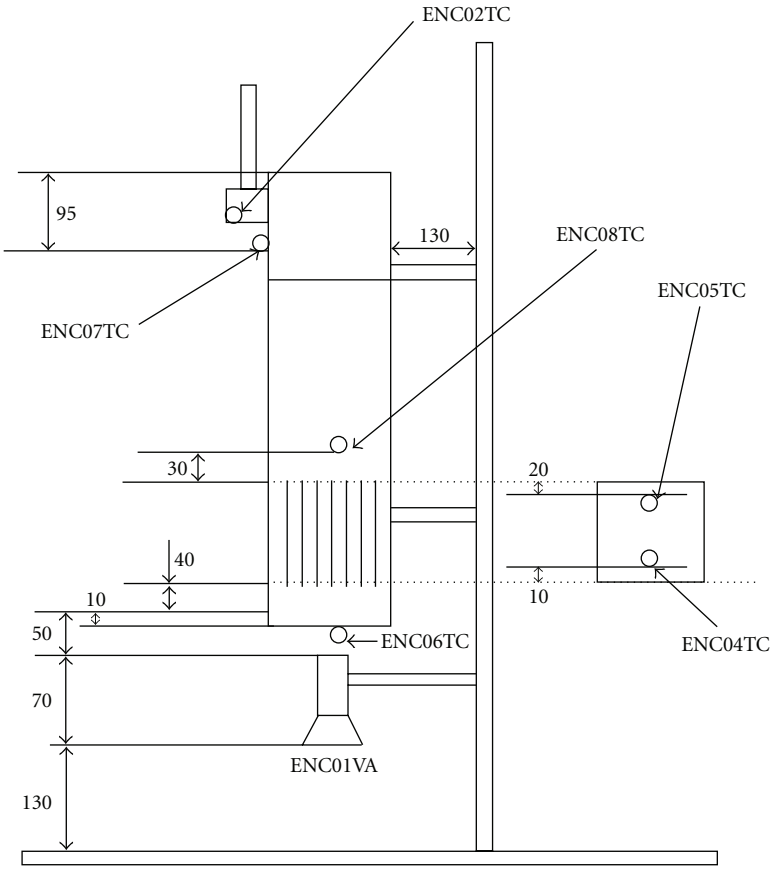

Figure 8: Sketch of KALI-H_2 test.

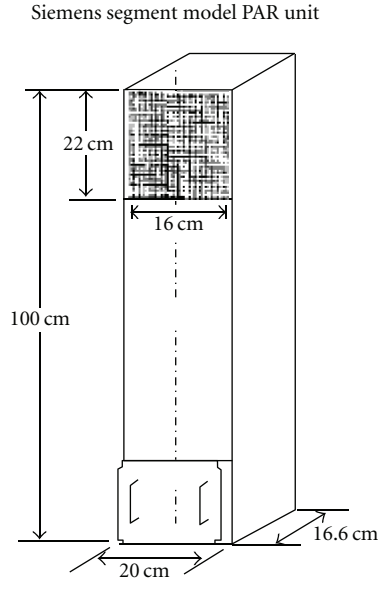

Figure 9: Sketch of PAR unit.

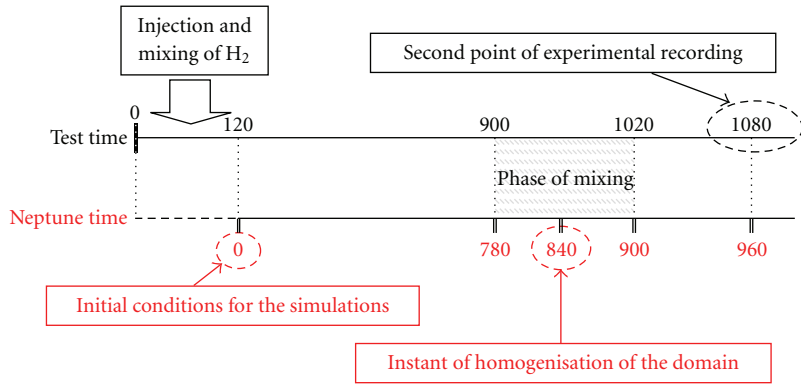

Figure 10: Stages, test number 008.

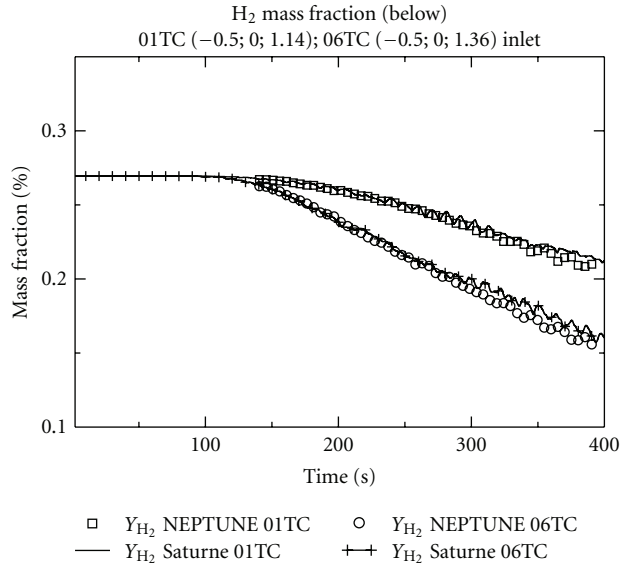

Figure 11: H_2 mass fraction below the PAR.

negligible regarding the effects of the fan device. In the following, the *k*-epsilon model is used in the calculations.

Figures 11 and 12 represent the hydrogen mass fraction below the recombiner and at the outlet of the recombiner, calculated with NEPTUNE_CFD and Code_Saturne. Results are similar which means PAR models are implemented in a similar way in both codes. As a consequence, NEPTUNE_CFD is indirectly checked against H_2-PAR test.

Figure 13 shows the time evolution of gas temperature at the outlet of the PAR. We observe large discrepancies between Code_Saturne and NEPTUNE_CFD after 300 s because the wall condensation effects and the heat exchange between the wall of vessel and the gas are not modelled in Code_Saturne in this calculation. Firstly, gas temperature decreases because of conduction inside the wall (heat and mass exchange). Secondly, vapour condensates at the wall which means that pressure decreases inside the vessel and thus the gas temperature decreases too because of the gas perfect law. Calculations and experimental data are in reasonable agreement.

Figure 14 represents the hydrogen molar fraction just below the recombiner. The dashed line is the result directly calculated. The continuous line takes into account a start-up delay time described in [3]. Avakian and Braillard have carefully studied the KALI-H_2 test and explain that the recombiner is wet because of the condensed team. Avakian has shown that the start-up delay time is between 1 to 6 min. Thus, numerical results compare favourably with experimental values.

Figure 15 shows gas temperature and hydrogen mass fraction fields in the computational domain. The heat of the reaction at the catalyst surface causes a buoyancy-induced flow accelerating the inflow rate. Figure 15 clearly underlines the influence of the PAR outflow on the mixing process.

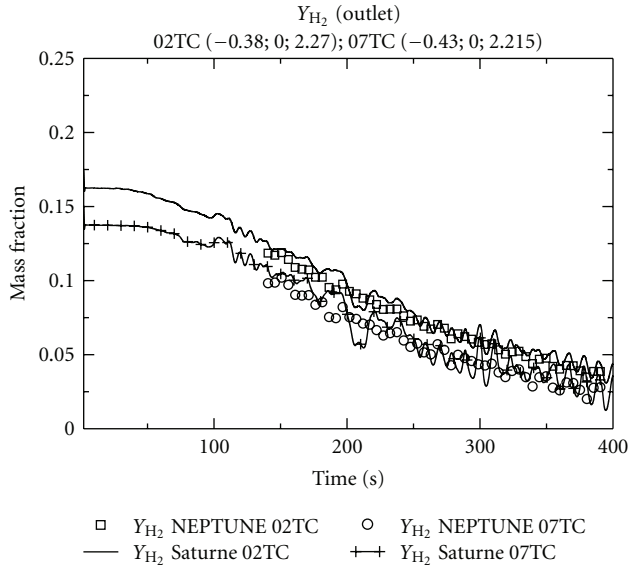

Figure 12: H_2 mass fraction at outlet of the PAR.

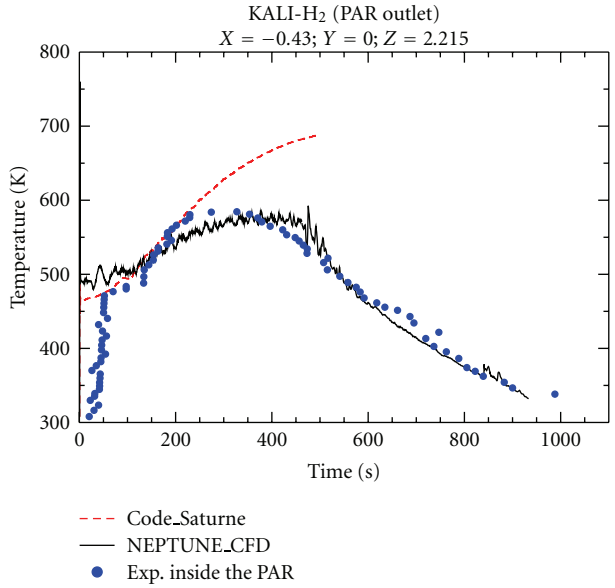

Figure 13: Time evolution of gas temperature at outlet of the PAR.

8. Conclusion

We have presented in this paper the models implemented in NEPTUNE_CFD, a three-dimensional two-fluid code dedicated to nuclear reactor applications and in Code_Saturne, a three-dimensional single-phase code. Thanks to a code-to-experiment benchmark based on the COPAIN and TOSQAN facilities [17], we successfully evaluated the ability of the code to reproduce the vapor condensation at wall, atmosphere mixing, and stratification in a vessel. These phenomena are of relevant interest in many industrial applications, especially regarding nuclear power plant containment at accident conditions. These models have been applied to the KALI-H_2 test. Moreover, PAR models have been tested against H_2-PAR and KALI-H_2 test and results are in a reasonable agreement with experimental values.

During the course of a severe accident in a pressurized water reactor (PWR), spray systems are used in a containment in order to limit overpressure, to enhance the gas mixing in case of the presence of hydrogen, and to drive down the fission products. Hence, vapor condensation on a cooled surface, spray effects, and PAR systems act simultaneously in applications which is made possible with the two-phase flow approach proposed in the paper.

The PAR models used in the paper are based on the manufacturer's correlation to calculate the hydrogen depletion rate. In future works, it would be interesting to test the impact of the correlation uncertainties on gas temperature

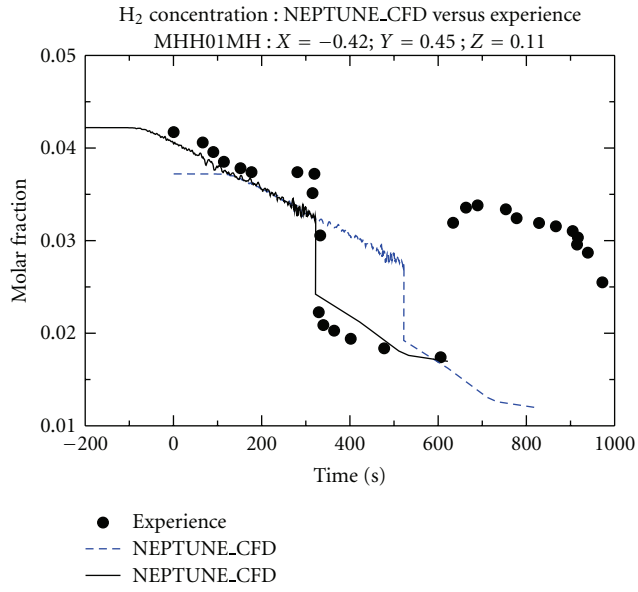

Figure 14: H_2 molar fraction just below the PAR.

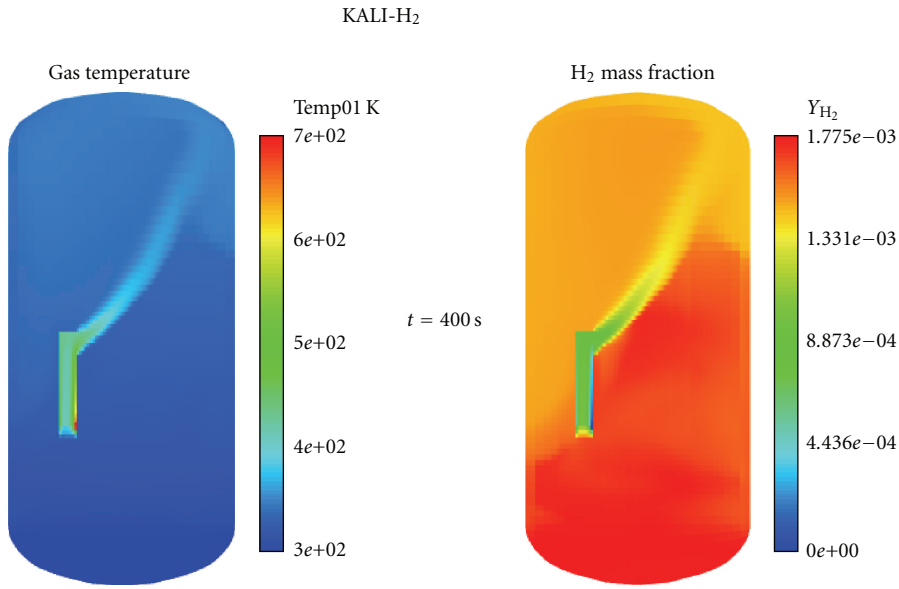

Figure 15: Gas temperature and hydrogen mass fraction fields.

and hydrogen mass fraction at the PAR outlet calculated by a CFD code. Comparisons between manufacturer's correlation and more sophisticated models based on gas phase and surface chemical mechanisms should be investigated.

Acknowledgments

This paper has been completed in the framework of the PAGODES2 project financially supported by EDF (Electricité de France). The NEPTUNE_CFD code is being developed in the framework of the NEPTUNE project financially supported by CEA (Commissariat à l'Energie Atomique), EDF (Electricité de France), IRSN (Institut de Radioprotection et de Sûreté Nucléaire), and AREVA-NP.

References

[1] O. Braillard et al., "Generic model tests of passive autocatalytic recombiners (PARs) for combustible gaz control in nuclear power plants," Technical note CEA Cadarache REF: EDF ND 1767, Volume 3, Test data for SIEMENS PARs.

[2] E. Bachellerie, F. Arnould, M. Auglaire et al., "Generic approach for designing and implementing a passive autocatalytic recombiner PAR-system in nuclear power plant containments," *Nuclear Engineering and Design*, vol. 221, no. 1–3, pp. 151–165, 2003.

[3] G. Avakian and O. Braillard, "Theorical model of hydrogen recombiner for a nuclear power plant," in *Proceedings of the 7th International Conference on Nuclear Engineering*, Tokyo, Japan, 1999.

[4] F. Fineschi, M. Bazzichi, and M. Carcassi, "A study on the hydrogen recombination rates of catalytic recombiners and deliberate ignition," *Nuclear Engineering and Design*, vol. 166, no. 3, pp. 481–494, 1996.

[5] J. Deng and X. W. Cao, "A study on evaluating a passive autocatalytic recombiner PAR-system in the PWR large-dry containment," *Nuclear Engineering and Design*, vol. 238, no. 10, pp. 2554–2560, 2008.

[6] S. Kudriakov et al., "The TONUS CFD Code for hydrogene risk analysis: physical models numerical schemes and validation matrix," in *Proceedings of the CFD for Nuclear Reactor Safety Applications Workshop (CFD4NRS '06)*, Garching, Germany, September 2006.

[7] S. Mimouni, M. Boucker, J. Laviéville, A. Guelfi, and D. Bestion, "Modelling and computation of cavitation and boiling bubbly flows with the NEPTUNE_CFD code," *Nuclear Engineering and Design*, vol. 238, no. 3, pp. 680–692, 2008.

[8] F. Archambeau, N. Méchitoua, and M. Sakiz, "Code_Saturne: a finite volume code for the computation of turbulent incompressible flows—industrial application," *International Journal on Finite Volumes*, vol. 1, 2004.

[9] M. Ishii, *Thermo-Fluid Dynamic, Theory of Two Phase*, Eyrolles, Collection de la Direction des Etudes et Recherches d'Electricité de France, 1975.

[10] A. Guelfi, D. Bestion, M. Boucker et al., "NEPTUNE: a new software platform for advanced nuclear thermal hydraulics," *Nuclear Science and Engineering*, vol. 156, no. 3, pp. 281–324, 2007.

[11] N. Mechitoua, J. Lavieville et al., "An unstructured finite volume solver for 2-phase water/vapor fows modelling based on an elliptic oriented fractional step method," in *Proceeding of the 10th International Topical Meeting on Nuclear Reactor Thermal Hydraulics (NURETH '03)*, Seoul, South Korea, October 2003.

[12] S. Mimouni, A. Foissac, and J. Lavieville, "CFD modelling of wall steam condensation by a two-phase flow approach ," *Nuclear Engineering and Design*. In Press.

[13] W. E. Ranz and W. R. Marschall, "Evaporation from drops," *Chemical Engineering Progress*, vol. 48, pp. 173–180, 1952.

[14] S. Mimouni, J.-S. Lamy, J. Lavieville, S. Guieu, and M. Martin, "Modelling of sprays in containment applications with a CMFD code," *Nuclear Engineering and Design*, vol. 240, no. 9, pp. 2260–2270, 2010.

[15] S. Bachere and F. Duplat, "MAAP code description and validation," Tech. Rep. ENTEAG030096A, Electricité de France, 2005.

[16] S. Mimouni, F. Archambeau, M. Boucker, J. Lavieville, and C. Morel, "A second order turbulence model based on a Reynolds stress approach for two-phase boiling flow and application to fuel assembly analysis," *Nuclear Engineering and Design*, vol. 240, no. 9, pp. 2225–2232, 2010.

[17] J. Malet, L. Blumenfeld, S. Arnd et al., "Sprays in containment: final results of the SARNET spray benchmark," in *Proceedings of the 3rd European Review Meeting on Severe Accident Research (ERMSAR '08)*, Nesseber, Bulgaria, September 2008.